



# Effect of Heat Treatment on the Microstructure, Mechanical Properties, and Corrosion Resistance of Friction Stir Processed Al-Zn-Mg-Cu-Sc-Zr Alloy

Y.F. Hou, J.J. Xiao, C.Y. Liu, and B. Zhang

Submitted: 21 October 2020 / Revised: 19 January 2021 / Accepted: 31 January 2021 / Published online: 9 April 2021

Post-heat treatment was conducted on the Al-Zn-Mg-Cu-Sc-Zr alloy treated by friction stir processing (FSP) to optimize its strength and corrosion resistance. Different post-heat routes had significant bearing on the phase composition of the FSP sample, while its fine equiaxed grain structure could be retained during post heating. Enhanced strength of the FSP sample was obtained by post-heat treatments. The FSP sample after T6 treatment (artificial aging to peak hardness value after solid solution treatment) exhibited the highest strength in virtue of its high precipitation strengthening effect, and the high ductility of the FSP sample could be retained after solid solution treatment. Furthermore, the FSP sample presented better corrosion resistance after artificial aging and T6 treatment by reducing its solution atom numbers.

**Keywords** Al-Zn-Mg-Cu-Sc-Zr alloy, friction stir processing, fine grain structure, heat treatment

## 1. Introduction

Friction stir process (FSP), which is one of the severe plastic deformation methods, is widely used in grain refinement of Al alloys (Ref 1-4). FSP Al alloys exhibit excellent characteristics, including superplasticity (Ref 5-8), high damping capacity (Ref 9, 10), and high corrosion resistance (Ref 11-13). However, the temperature rise during FSP decreases the strength of the FSP Al alloys (Ref 14, 15).

Kumar et al. (Ref 16) found that additional cooling during FSP could further refine the grains of FSP 7075 Al alloy and then improve its mechanical properties. Post-heat treatment was also adopted to improve the alloy strength. Zeng et al. (Ref 17) and Gholami et al. (Ref 18) found that the strength of FSP Al alloys can be enhanced by performed artificial aging (AA) due to the precipitation of metastable phase during this process. Solid solution (ST) before AA can further enhance the density of metastable phase, and the strength of FSP Al alloys may also be enhanced by T6 treatment (AA to peak hardness value after ST). However, abnormal grain growth of fine grains in FSP Al alloys is hard to avoid during ST treatment (Ref 19), and the excellent characteristics of Al alloys with fine grain structure, such as excellent corrosion resistance, may be worsened by grain coarsening.

Charit et al. (Ref 20) and Liu et al. (Ref 21) added Sc into Al-Zn-Mg-Cu-Zr alloys and found that the grain structure in

these FSP Al alloys exhibits excellent thermal stability during T6 treatment owing to the existence of nanosized  $Al_3(Sc,Zr)$  phases and their grain boundary (GB) pinning effect. Therefore, for FSP aluminum alloys added with Sc, post-T6 treatment could also be used to enhance their strength without severely sacrificing their other characteristics. However, the effect of post-heat treatment route such as AA, ST, and T6 on the mechanical properties of FSP Al alloys has not been studied systematically yet. Furthermore, the corrosion resistance of the fine grain structure Al-Zn-Mg-Cu-Zr alloys was also affected by their precipitates density, distribution, and size. Thus, the effect of post-heat treatment route on the corrosion resistance of FSP Al alloys should be also studied.

In this paper, the effects of three post-heat treatment methods, including AA, ST, and T6, on the microstructure, mechanical properties, and corrosion resistance of the FSP Al-Zn-Mg-Cu-Sc-Zr alloy were compared. This study aimed to fabricate high-strength FSP Al alloys using post-heat treatment without sacrificing their outstanding corrosion resistance.

## 2. Experimental Procedures

The Al-8.24Zn-1.7Mg-1.66Cu-0.25Sc-0.15Zr (7085 with 0.25 wt.% Sc addition) alloy after FSP (traverse speed: 100 mm/min, tool rotation rate: 800 rpm, concave shoulder diameter: 16 mm, tapered threaded pin diameter: varied from 3.5 mm to 5.5 mm, and pin long: 3.8 mm) was used as raw material, and Fig. 1 shows the macrostructure of FSP zone. Three heat treatment routes were performed on the FSP samples: (1) aging, 393 K, till peak hardness value, (2) solid solution, 743 K, 1 h, and (3) route (2) + route (1), with the sample name of AA-FSP, ST-FSP, and T6-FSP, respectively. A Vickers microhardness tester (Leco-LM 248AT) was used to measure the hardness of samples that underwent aging, and then, the aging parameters of aged samples were confirmed by the age-hardening curves.

An FEI Tecnai G2 F20 S-TWIN transmission electron microscopy (TEM) and the electron backscatter diffraction

Y.F. Hou, J.J. Xiao, and C.Y. Liu, Key Laboratory of New Processing Technology for Nonferrous Metal and Materials, Ministry of Education, Guilin University of Technology, Guilin 541004, China; and B. Zhang, State Key Laboratory of Metastable Materials Science and Technology, Yanshan University, Qinhuangdao 066004, China. Contact e-mails: ley261@glut.edu.cn and zhangbing@ysu.edu.cn.

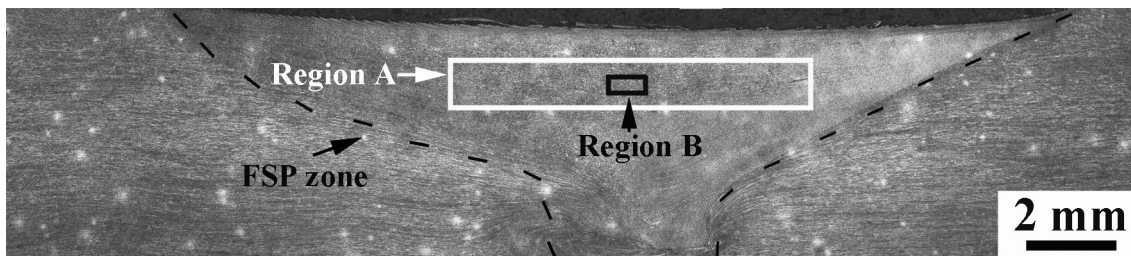


Fig. 1 Macrostructure of FSP zone

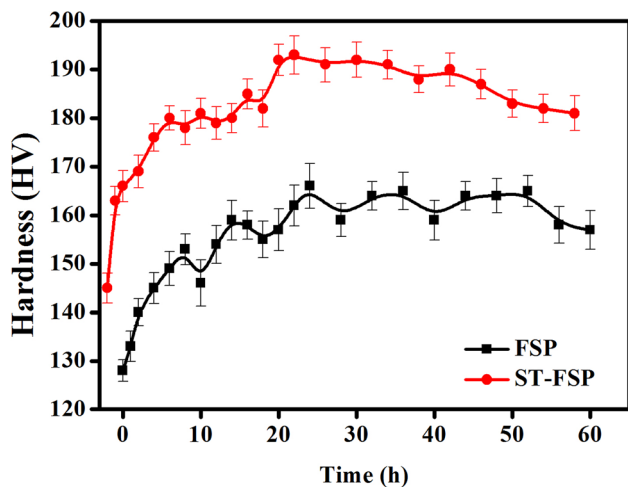


Fig. 2 Age-hardening curves of different samples

(EBSD, EDAX system) were utilized to obtain the microstructure of samples. The operating voltages of the TEM test were 200 kV. EBSD analysis was conducted using a scanning electron microscope (Hitachi S-3400 N) with EDAX system. The operating voltage and working distance were 20 kV and 15 mm, respectively, and the scan step size of mapping was 0.3  $\mu\text{m}$ .

The tensile properties of samples were obtained on an Instron-8801 mechanical testing machine with the strain rate was  $4 \times 10^{-4} \text{ s}^{-1}$ . The 3 tensile specimens were prepared according to the inset of Fig. 7, and the tensile test adopted the standard of ASTM: E8/E8M-11. The corrosion resistance of samples was evaluated through the intergranular corrosion (IGC) test and carried out according 7998-2005 GB/T standard. The solution used in the IGC test contained 57 g NaCl, 10 mL  $\text{H}_2\text{O}_2$ , and 1 L distilled water. The IGC test temperature and time were 298 K and 24 h, respectively. The depth of corrosion damage of samples was examined on a Leica-DMi8 optical microscopy (OM).

“Region A” in Fig. 1 was the place for tensile test, and “Region B” in Fig. 1 was the place for TEM, EBSD, hardness, and corrosion resistance tests.

### 3. Results

The age-hardening curves of different samples are showed in Fig. 2. The original hardness of the ST-FSP sample was 145 HV, higher than the original hardness of the FSP sample (128 HV). Both the ST-FSP and FSP samples could be hardened by

aging, reaching their peak hardness values at 24 h. The peak hardness value of the T6-FSP (193 HV) was obviously higher compared to the AA-FSP sample (166 HV).

The EBSD maps of different samples are presented in Fig. 3. The FSP sample exhibits a typical fine equiaxed grain structure (Fig. 3a), and no alteration occurs to the grain structure of FSP samples after heat treatments (Fig. 3b-d).

The grain size distributions and the average grain size (AGS) of samples are displayed in Fig. 4. The AGS of the FSP sample was 4.3  $\mu\text{m}$  with the largest grain size of 8  $\mu\text{m}$  (Fig. 4a). Heat treatment coarsened the grains of the FSP sample, and the largest grains in all heat-treated samples were larger than 10  $\mu\text{m}$  (Fig. 4). The AGSs of AA-FSP sample, ST-FSP sample, and T6-FSP sample were 4.4, 4.4, and 4.5  $\mu\text{m}$ , respectively.

The TEM images of the FSP sample can be seen in Fig. 5. Rod-like phases with hundreds of nanometers in length were observed in the grains, and fine equiaxed phase with several nanometers in diameter could be observed on some rod-like phases. Energy dispersive spectroscopy showed that the rod-like phase and the equiaxed phase were  $\eta$  phase and  $\text{Al}_3(\text{Sc,Zr})$  phase, respectively. In the FSP sample, the  $\eta$  phases at GB significantly larger than intragranular phase in size could also be observed, and these phases exhibited a discontinuous distribution along the GBs (Fig. 5a), while no nanosized precipitated phase could be found (Fig. 5b).

The TEM images of the FSP sample after post-heat treatments are pasted in Fig. 6. Aging resulted in the precipitation of  $\eta'$  phase (Fig. 6b) without altering the distribution and size of the  $\eta$  phases of the FSP sample (Fig. 6a). Furthermore, a 100 nm wide precipitate-free zone (PFZ) could be seen near the grain boundaries of the AA-FSP sample.

Both the ST-FSP sample and the T6-FSP sample were observed with the disappearance of the intragranular  $\eta$  phases but the existence of  $\text{Al}_3(\text{Sc,Zr})$  phases (Fig. 6c and e). As shown in Fig. 6(d), GB phases with continuous distribution could be obtained in the ST-FSP sample. In the T6-FSP sample (Fig. 6f), the GB phases exhibited a discontinuous distribution along the GBs, and PFZ with the width of 20 nm and nanosized precipitated phase with high density could be observed. High-resolution TEM showed that these phases were  $\eta'$  phases (Fig. 6f).

The stress-strain relationships of different samples are shown in Fig. 7. The yield strength (YS), ultimate tensile strength (UTS), and elongation (EL) of the FSP sample were, respectively, 300 MPa, 410 MPa, and 28%. The three post-heat treatment methods could enhance the strength of the FSP alloy. The T6-FSP sample possessed higher YS and UTS (up to 511 MPa and 559 MPa, respectively) but lower EL (19%) than the other two post-heat-treated samples. Compared with the ST-FSP sample, the AA-FSP sample has higher YS but lower UTS.



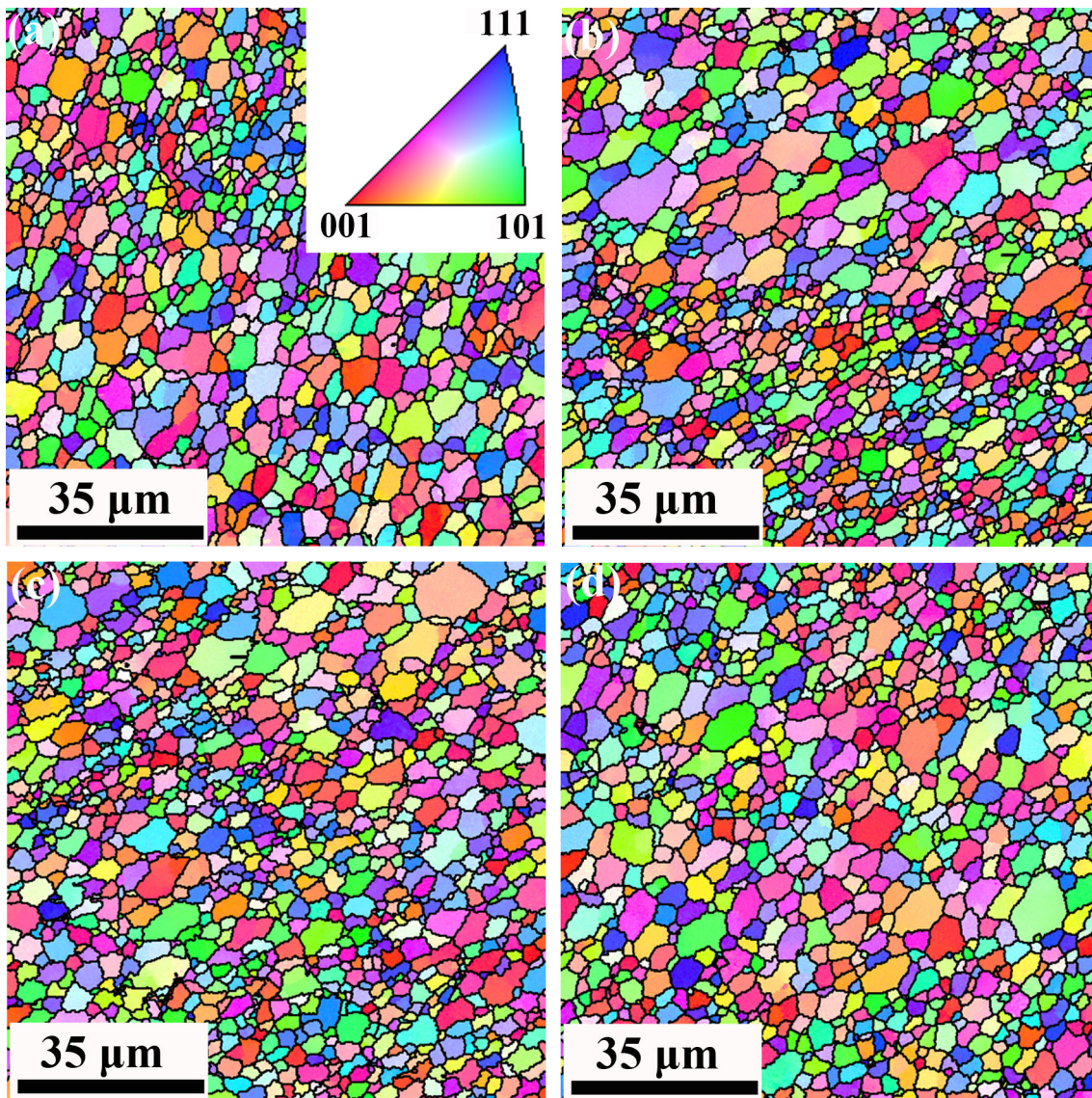


**Fig. 3** EBSD maps of different samples: (a) FSP, (b) AA-FSP, (c) ST-FSP, and (d) T6-FSP

The EL of the ST-FSP sample remained almost the same as that of the FSP sample.

The OM images of samples after IGC test for 24 h are illustrated in Fig. 8. The deepest damage of the FSP sample was  $38.8 \mu\text{m}$  (Fig. 8a). According to Fig. 8(b and e), the maximum damage depths decreased to  $32.6$  and  $28.8 \mu\text{m}$  after AA and T6 treatments, respectively, showing that both treatments slightly improved the corrosion resistance of the FSP sample. The ST-FSP sample was observed with the maximum damage depth of as high as  $320 \mu\text{m}$  (Fig. 8c), revealing the corrosion resistance of the FSP sample was obviously worsened by ST treatment. The GBs provided corrosion channels during the IGC process (Fig. 8d).

#### 4. Discussion

Nanosized  $\text{Al}_3(\text{Sc,Zr})$  particles exist in Al alloys added with Sc, and these particles can pin the GBs of Al alloys during heat treatments (Ref 22-25). The GBs of FSP sample can also be

pinned by  $\text{Al}_3(\text{Sc,Zr})$  particles in the process of post-heat treatment, even when the temperature reaches  $743 \text{ K}$  (Ref 20, 21). Thus, after all the three post-heat treatments of AA, ST and T6, the fine equiaxed grains were still well kept in the sample (Fig. 3 and 4).

The  $\eta$  phases precipitated during FSP, and the GBs promoted this precipitation behavior. Thus, the GB phases were larger than the intragranular  $\eta$  phases (Fig. 5a). Furthermore, the  $\text{Al}_3(\text{Sc,Zr})$  particles acted as heterogeneous nucleation points for the  $\eta$  phases, and they can be observed on some  $\eta$  phases (Fig. 5a).

The age-hardening behavior of the FSP sample (Fig. 2) indicates that this sample contains some solution atoms, and aging brought about the formation of  $\eta'$  phases. However, the low temperature of aging could prevent the phase evolution of  $\eta$  phases. Thus, high densities of  $\eta'$  phase and  $\eta$  phase were in view in the AA-FSP sample (Fig. 6a and b). The large GB phase consumed a great quantity of Mg and Zn atoms, thereby leading to the formation of PFZ in the AA-FSP sample.

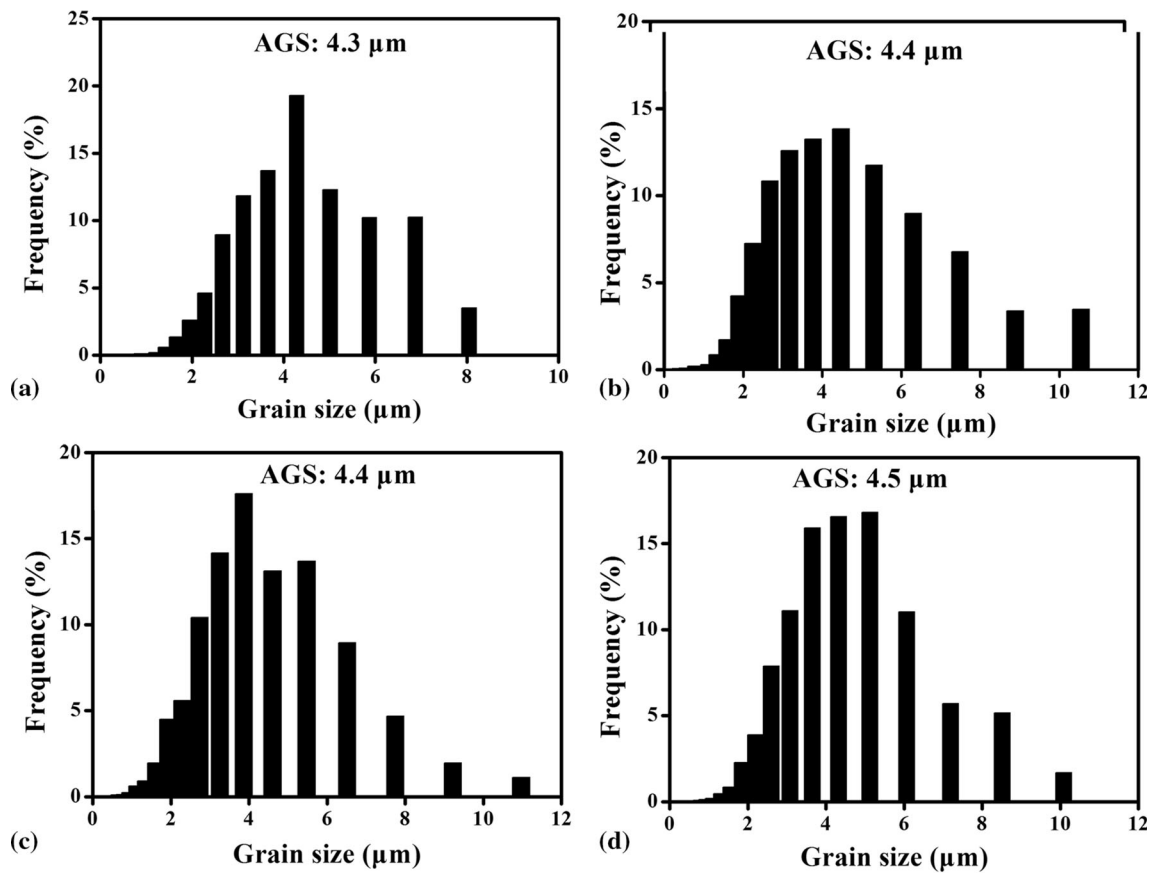


**Fig. 4** Grain size distribution and AGS of different samples: (a) FSP, (b) AA-FSP, (c) ST-FSP, and (d) T6-FSP

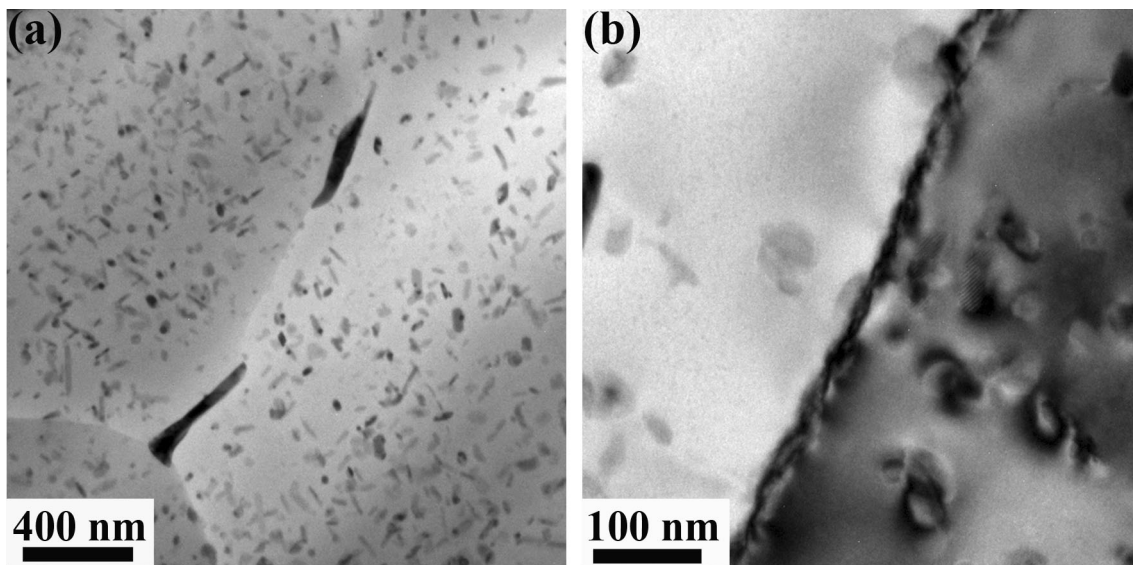


**Fig. 5** FSP sample TEM images: (a) low-magnification, (b) high-magnification

The  $\eta$  phases in the FSP sample were dissolved after ST treatment, and the high energy promoted the precipitation of GB phases after solution treatment. Thus, the density of intragranular precipitates in the ST-FSP sample was lower than that in the FSP sample, and continuous GB phases were got in the ST-FSP sample (Fig. 6c and d). The solution atoms in the ST-FSP sample re-precipitated and then formed high density of

$\eta'$  phases during aging. Thus, the  $\eta'$  phases in the T6-FSP sample were of high density. The fine GB phases merged, and more solution atoms spread to GBs in the ST-FSP sample during aging. Thus, GB phases with discontinuous distribution and PFZ could be obtained after T6 treatment (Fig. 6f). The GB phases in the T6-FSP sample were much finer than those in the AA-FSP sample. This means that less solution atoms were



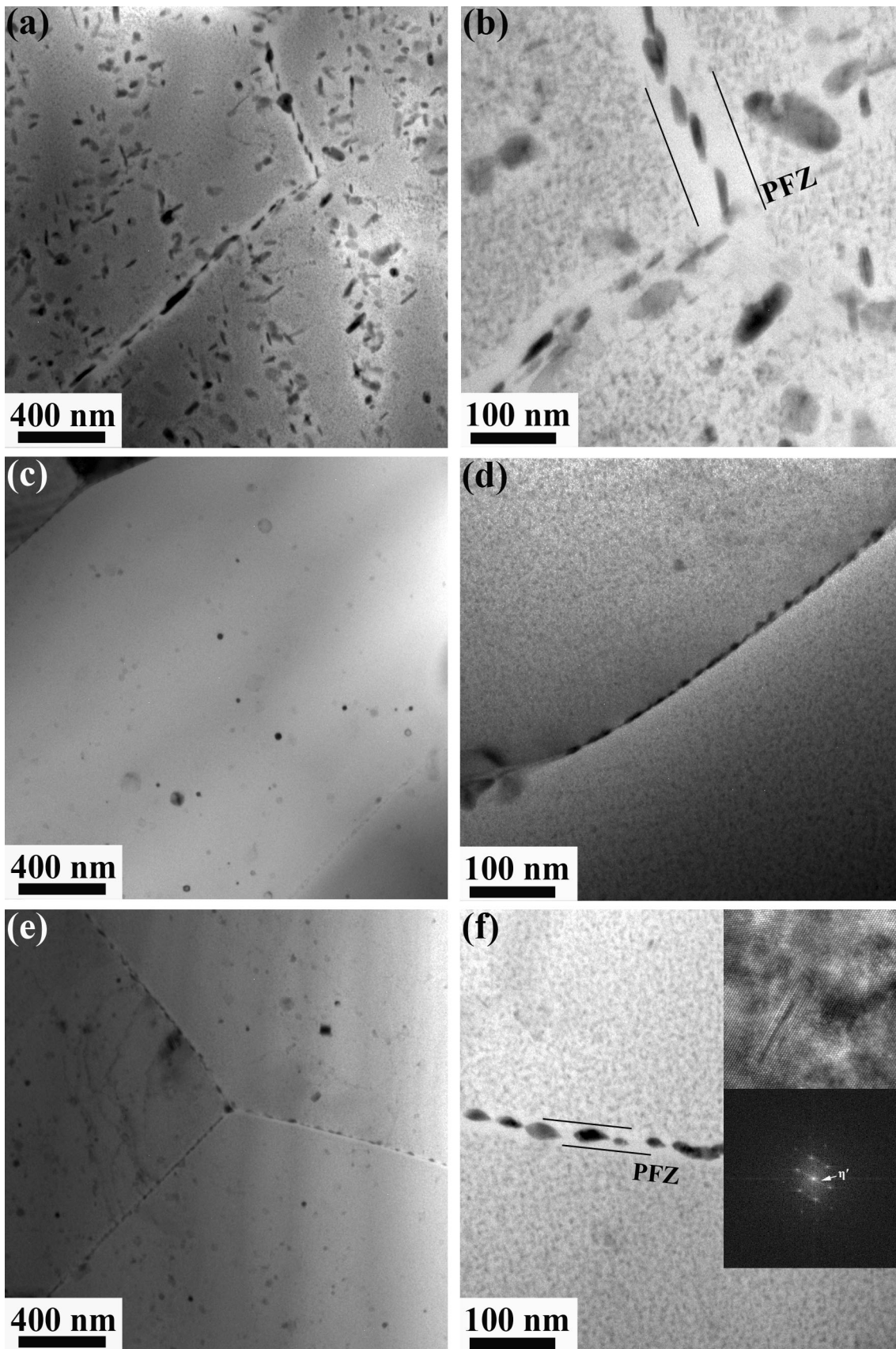


**Fig. 6** TEM images of (a, b) AA-FSP, (c, d) ST-FSP, and (e, f) T6-FSP samples: (a), (c), (e) low-magnification; (b), (d), (f) high-magnification

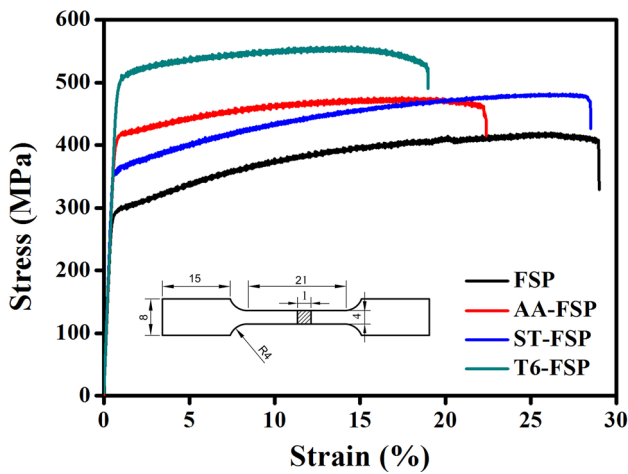


Fig. 7 Stress-strain curves of different samples

consumed by the GBs in the T6-FSP sample so that it had much narrower PFZ than the AA-FSP sample.

Heat treatment did not significantly change the grain shape and grain size of the FSP sample (Fig. 3 and 4). Thus, the difference of GB strengthening effect of the four samples in this study can be neglected. The mechanical properties of samples mainly depended on their phase compositions.

Aging caused the precipitation of  $\eta'$  phases, so as to reinforce the precipitation strengthening of Al alloys. Thus, the strength of different samples exhibited the relationships: AA-FSP higher than FSP and T6-FSP higher than ST-FSP. The  $\eta$  phase in the AA-FSP sample consumed some solution atoms, and the AA-FSP sample contained less  $\eta'$  phases compared to T6-FSP sample. Therefore, the T6-FSP sample possessed higher precipitation strengthening effect, resulting in its higher strength compared with the AA-FSP sample. The  $\eta$  phases in the FSP sample dissolved into Al lattice during ST treatment. Thus, the ST-FSP sample possessed higher solution strengthening effect, resulting in its higher strength than the FSP sample. However, the solution strengthening effect is much lower than the precipitation strengthening effect for Al alloys. Thus, the YS of the AA-FSP sample was higher than that of the ST-FSP sample although only part of solution atoms changed to  $\eta'$  phases in the AA-FSP sample.

The solution atoms can impede the movement of dislocation in the Al alloys during tension test and then increase the dislocation accumulation ability of Al alloys. Thus, the work hardening rate of the ST-FSP sample exceeded that of the AA-FSP sample (Fig. 7) and thereby exhibiting the following UTS relationship: ST-FSP > AA-FSP. The high work hardening rate also improved the ductility of Al alloys. Thus, the EL of the ST-FSP sample was higher than the rest two heat-treated FSP samples.

For the Al alloy friction stir welding (FSW) joint, the fine equiaxed grain structures in the stir zones issued in the satisfactory corrosion resistance (Ref 11, 13, 26). In this study,

the FSP sample also displayed satisfactory anti-corrosion property with the maximum damage depth after IGC test for 24 h of only 38.8  $\mu\text{m}$  (Fig. 7a). The solution atoms are important promoters of the corrosion acceleration of Al alloys (Ref 27). The solution atoms in the FSP sample were consumed during aging, and the solution atom numbers of the FSP sample were increased by ST treatment. Thus, the corrosion resistance exhibited the relationship of AA-FSP > FSP > ST-FSP (Fig. 8a-c). Furthermore, the continuously distributed GB phases could provide corrosion channels during the IGC test (Ref 28) and then promoted the IGC of the ST-FSP sample (Fig. 8d).

The T6-FSP sample was also characterized by low content of solution atoms and its corrosion resistance was higher than the FSP and ST-FSP samples (Fig. 8e). Although also exhibiting a low content of solution atoms, the corrosion resistance of the AA-FSP sample was below the T6-FSP sample due to the narrower PFZs in T6-FSP sample (Ref 29). Thus, the T6-FSP sample was crowned the optimum corrosion resistance among all samples.

## 5. Conclusions

This paper investigated the influence of different post-heat treatments on the microstructure, mechanical properties, and corrosion resistance of FSP Al-Zn-Mg-Cu-Sc-Zr alloy. Here, summarize the conclusions as below:

1. On account of the pinning effect of  $\text{Al}_3(\text{Sc,Zr})$  particles, the fine equiaxed grain structure of the FSP sample was well retained during post heating.
2. Aging led to the  $\eta'$  phase precipitation without altering the distribution and size of the  $\eta$  phases in the FSP sample, ST treatment caused the  $\eta$  phase dissolution in the FSP sample, and T6 treatment brought about high-density  $\eta'$  phase. The GB promoted the precipitation behavior during heat treatment, and the PFZ can be obtained in the aged samples.
3. The FSP sample strength was enhanced by post-heat treatment, and the high precipitation strengthening effect of the T6-FSP sample brought it the highest strength. Attributed to the high numbers of solution atoms of the ST treatment, the AT-FSP sample exhibited a high ductility with the EL of up to 28%.
4. The post-aging treatment and the post-T6 treatment improved the corrosion resistance of FSP sample by decreasing its solution atom numbers, and the T6-FSP sample showed better anti-corrosion property than the AA-FSP sample due to its narrower PFZs. The ST-FSP sample was easier corrosive than the FSP sample owing to its high numbers of solution atoms and GB phases with continuous distribution.



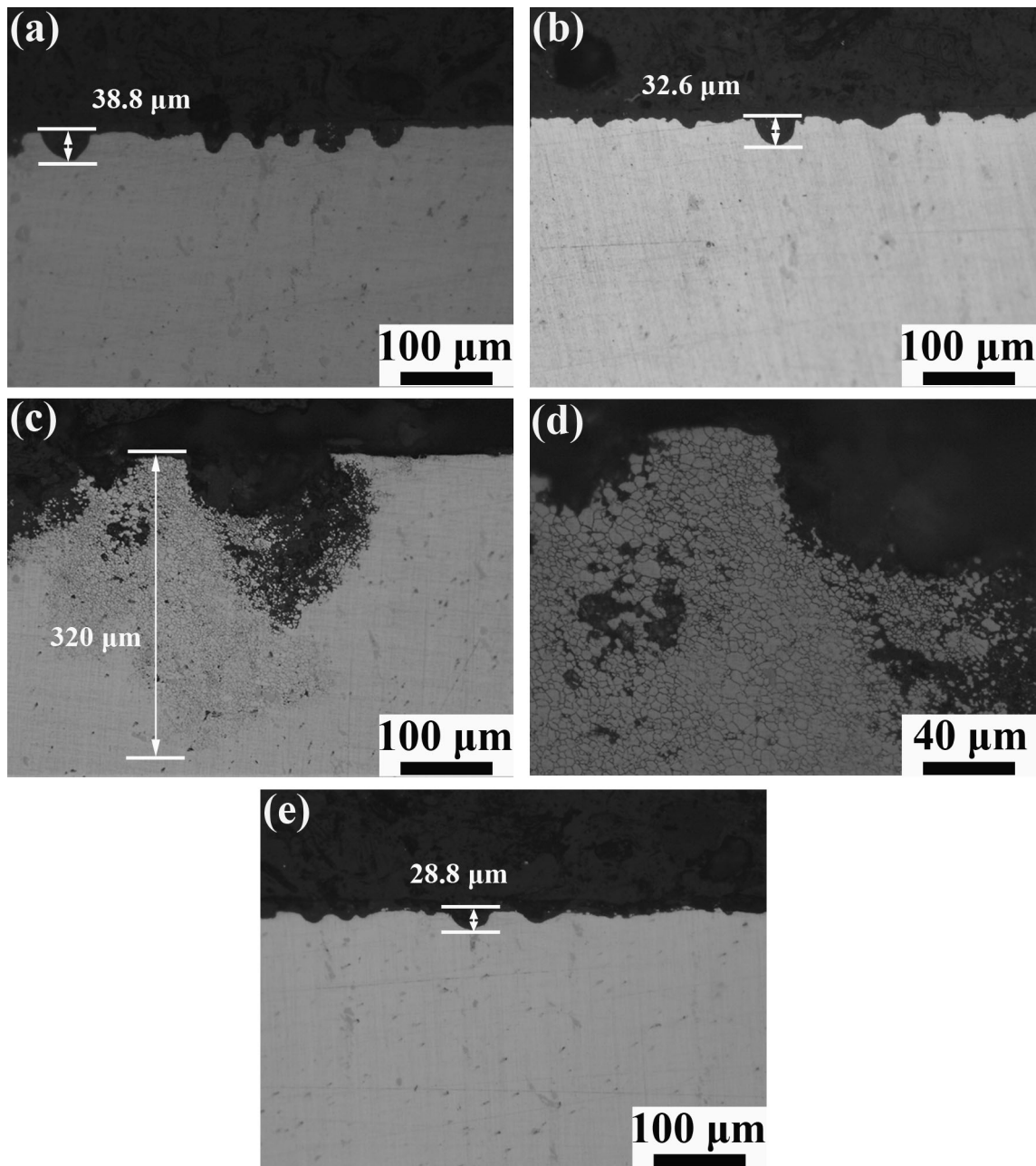


**Fig. 8** OM images of different samples after IGC for 24 h: (a) FSP, (b) AA-FSP, (c) (d) ST-FSP, and (e) T6-FSP

### Acknowledgments

This work was funded by the Science and Technology Major Project of Guangxi (Grant No. GKAA17202007)

### References

1. R.S. Mishra and Z.Y. Ma, Friction Stir Welding and Processing, *Mater. Sci. Eng. R*, 2005, **50**, p 1–78
2. Z.Y. Ma, Friction Stir Processing Technology: A Review, *Metall. Mater. Trans.*, 2008, **39**, p 642–658
3. Y.Y. Hu, H.J. Liu, H. Fujii, H. Araki, K. Sugita and K. Liu, Ultrasonic-Induced Excess Vacancies in Friction Stir Processing and Exploration of Acoustoplastic Effect, *Scripta Mater.*, 2020, **185**, p 117–121
4. V. Kulitskiy, S. Malopheyev, S. Mironov and R. Kaibyshev, Grain Refinement in an Al-Mg-Sc Alloy: Equal Channel Angular Pressing Versus Friction-Stir Processing, *Mater. Sci. Eng. A*, 2016, **674**, p 480–490
5. I. Charit and R.S. Mishra, low Temperature Superplasticity in a Friction-Stir-Processed Ultrafine Grained Al-Zn-Mg-Sc Alloy, *Acta Mater.*, 2005, **53**, p 4211–4223
6. F.C. Liu and Z.Y. Ma, Low-Temperature Superplasticity of Friction Stir Processed Al-Zn-Mg-Cu Alloy, *Scripta Mater.*, 2008, **58**, p 667–670
7. A. Orozco-Caballero, O.A. Ruano, E.F. Rauch and F. Carreño, Severe Friction Stir Processing of an Al-Zn-Mg-Cu Alloy: Misorientation and Its Influence on Superplasticity, *Mater. Des.*, 2018, **137**, p 128–139
8. Z.Y. Ma, F.C. Liu and R.S. Mishra, Superplastic Deformation Mechanism of An Ultrafine-Grained Aluminum Alloy Produced by Friction Stir Processing, *Acta Mater.*, 2010, **58**, p 4693–4704
9. C.Y. Liu, H.J. Jiang, B. Zhang and Z.Y. Ma, High Damping Capacity of Al Alloys Produced by Friction Stir Processing, *Mater. Charact.*, 2018, **136**, p 382–387
10. H.J. Jiang, B. Zhang, C.Y. Liu, Z.X. Yang and Z.Y. Ma, Mechanical and Damping Behavior of Age-Hardened and Non-Age-Hardened Al

- Alloys After Friction Stir Processing, *Acta Metall. Sin. (English letters)*, 2019, **32**, p 1135–1141
11. N.D. Nam, L.T. Dai, M. Mathesh, M.Z. Bian and V.T.H. Thu, Role of Friction Stir welding-Traveling Speed in Enhancing the Corrosion Resistance of Aluminum Alloy, *Mater. Chem. Phys.*, 2016, **173**, p 7–11
  12. J.J. Pang, F.C. Liu, J. Liu, M.J. Tan and D.J. Blackwood, Friction stir processing of aluminium alloy AA7075: Microstructure, surface chemistry and corrosion resistance, *Corrosion Sci.*, 2016, **106**, p 217–228
  13. S. Sinhmar and D.K. Dwivedi, A Study on Corrosion Behavior of Friction Stir Welded and Tungsten Inert Gas Welded AA2014 Aluminium Alloy, *Corrosion Sci.*, 2018, **133**, p 25–35
  14. R. Abrahams, J. Mikhail and P. Fasihi, Effect of Friction Stir Process Parameters on the Mechanical Properties of 5005–H34 and 7075–T651 Aluminium Alloys, *Mater. Sci. Eng. A*, 2019, **751**, p 363–373
  15. H.L. Zhao, Q. Pan, Q.D. Qin, Y.J. Wu and X.D. Su, Effect of the Processing Parameters of Friction Stir Processing on the Microstructure and Mechanical Properties of 6063 Aluminum Alloy, *Mater. Sci. Eng. A*, 2019, **751**, p 70–79
  16. A. Kumar, A.K. Godasu, K. Pal and S. Mula, Effects of in-Process Cryocooling on Metallurgical and Mechanical Properties of Friction Stir Processed Al7075 Alloy, *Mater. Charact.*, 2018, **144**, p 440–447
  17. X.H. Zeng, P. Xue, L.H. Wu, D.R. Ni, B.L. Xiao and Z.Y. Ma, Achieving an Ultra-High Strength in a Low Alloyed Al Alloy Via a Special Structural Design, *Mater. Sci. Eng. A*, 2019, **755**, p 28–36
  18. S. Gholami, E. Emadoddin, M. Tajally and E. Borhani, Friction Stir Processing of 7075 Al Alloy and Subsequent Aging Treatment, *Trans. Nonferrous Metals Soc. China*, 2015, **25**, p 2847–2855
  19. I. Charit and R.S. Mishra, Abnormal Grain Growth in Friction Stir Processed Alloys, *Scripta Mater.*, 2008, **58**, p 367–371
  20. I. Charit and R.S. Mishra, Effect of Friction Stir Processed Microstructure on Tensile Properties of an Al-Zn-Mg-Sc Alloy Upon Subsequent Aging Heat Treatment, *J. Mater. Sci. Technol.*, 2018, **34**, p 214–218
  21. C.Y. Liu, B. Zhang, Z.Y. Ma, H.J. Jiang and W.B. Zhou, Effect of Sc Addition, Friction Stir Processing, and T6 Treatment on the Damping and Mechanical Properties of 7055 Al Alloy, *J. Alloy Compd.*, 2019, **772**, p 775–781
  22. K.X. Wang, D.F. Yin, Y.C. Zhao, A. Atrens and M.C. Zhao, Microstructural Evolution Upon Heat Treatments and Its Effect on Corrosion in Al-Zn-Mg Alloys Containing Sc and Zr, *J. Mater. Res. Technol.*, 2020, **9**, p 5077–5089
  23. J. Ren, R.C. Wang, Y. Feng, C.Q. Peng and Z.Y. Cai, Microstructure Evolution and Mechanical Properties of an Ultrahigh Strength Al-Zn-Mg-Cu-Zr-Sc (7055) Alloy Processed by Modified Powder Hot Extrusion with Post Aging, *Vacuum*, 2019, **161**, p 434–442
  24. J. Liu, P. Yao, N.Q. Zhao, C.S. Shi, H.J. Li, X. Li, D.S. Xi and S. Yang, Effect of Minor Sc and Zr on Recrystallization Behavior and Mechanical Properties of Novel Al-Zn-Mg-Cu Alloys, *J. Alloy Compd.*, 2016, **657**, p 717–725
  25. Y. Chen, C.Y. Liu, B. Zhang, Y.F. Hou and Z.Z. Xu, Effects of Mg and Sc Additions on the Microstructure and Mechanical Properties of Al-20Zn Alloys, *Mater. Charact.*, 2020, **159**, p 110000
  26. Y. Chen, Y.Q. Wang, L. Zhou, G.Z. Meng, B. Liu, J.Y. Wang, Y.W. Shao and J.T. Jiang, Macro-Galvanic Effect and Its Influence on Corrosion Behaviors of Friction Stirwelding Joint of 7050–T76 Al Alloy, *Corrosion Sci.*, 2020, **164**, p 108360
  27. S.Y. Chen, K.H. Chen, G.S. Peng, L. Jia and P.X. Dong, Effect of Heat Treatment on Strength, Exfoliation Corrosion and Electrochemical Behavior of 7085 Aluminum Alloy, *Mater. Des.*, 2012, **35**, p 93–98
  28. W.C. Yang, S.X. Ji, Q. Zhang and M.P. Wang, Investigation of Mechanical and Corrosion Properties of an Al-Zn-Mg-Cu Alloy Under Various Ageing Conditions and Interface Analysis of  $\eta$ 0 Precipitate, *Mater. Des.*, 2015, **85**, p 752–761
  29. L. Liu, Y.Y. Jia, J.T. Jiang, B. Zhang, G.A. Li, W.Z. Shao and L. Zhen, The Effect of Cu and Sc on the Localized Corrosion Resistance of Al-Zn-Mg-X Alloys, *J. Alloys Compd.*, 2019, **799**, p 1–14

**Publisher's Note** Springer Nature remains neutral with regard to jurisdictional claims in published maps and institutional affiliations.